THE ASTROPHYSICAL JOURNAL, 430:690–705, 1994 August 1

HIGH RYDBERG STATE CARBON RECOMBINATION LINES TOWARD CASSIOPEIA A: PHYSICAL CONDITIONS AND A NEW CLASS OF MODELS

H. E. PAYNE
Space Telescope Science Institute, 3700 San Martin Drive, Baltimore, MD 21218
K. R. ANANTHARAMAIAH
Raman Research Institute, Bangalore 560 080, India
AND
W. C. ERICKSON
Physics Department, University of Tasmania, Box 252C, GPO Hobart, Tasmania 7001, Australia
Received 1993 April 30; accepted 1994 January 26

ABSTRACT

We present models of physical conditions in Perseus arm clouds observed in the direction of Cas A. Theoretical predictions of carbon radio recombination line intensities are compared with observations spanning the frequency range 14–775 MHz. Best-fitting model parameters are then combined with the results of λ21 cm H I absorption line observations, and low-frequency hydrogen recombination line observations, to evaluate the thermal and pressure balance in these clouds. A critical reexamination of the available recombination line data shows that the lowest frequency carbon line observations have underestimated the integrated optical depths in the line by up to a factor of 3. This is due to the removal of large Lorentzian wings from the pressure-broadened line profiles during baseline subtraction. Models where some or all of the recombination line optical depth originates in molecular clouds do not give satisfactory results. Models based on standard calculations of recombination line intensities (Salem & Brocklehurst 1979; Walmsley & Watson 1982) have high pressures and are out of thermal balance.

We modified the theoretical calculation of line intensities, described by Salem & Brocklehurst (1979) and Walmsley & Watson (1982), by imposing a different boundary condition at large principal quantum number n. Instead of assuming an infinite number of levels populated according to thermodynamic equilibrium, we impose a cutoff in level populations above a critical principal quantum number n_{cr}, as suggested by Gulyaev & Nefedov (1989). We followed the occupation probability formalism presented by Hummer & Mihalas (1988) to calculate n_{cr}.

Using these new line intensity calculations, we find that, with the exception of the recombination line width, all of the Cas A recombination line and λ21 cm H I absorption line data can be attributed to a region where the physical conditions are typical of the cold neutral medium of the interstellar medium. We show a model in which this region is in thermal balance at a temperature near 36 K and has a reasonable interstellar pressure. In this model, the photoionization of polycyclic aromatic hydrogen molecules is the dominant mechanism for heating the region.

Subject headings: atomic processes — ISM: abundances — line: formation — radio lines: ISM

1. INTRODUCTION

The line of sight to the strong radio source Cas A, which intersects the Perseus and the Orion arms, has provided a uniquely detailed set of observations of radio recombination lines from highly excited states of singly ionized carbon ions. A large body of recombination line data has been obtained toward this direction at a number of frequencies. Observed principal quantum number range from $n = 166$ to $n = 766$. Very low frequency observations (14.7–30 MHz) have been performed by Konovalenko & Sodin (1980, 1981) and Konovalenko (1984, 1990) using the UTR2 radio telescope near Kharkov, Ukraine. Intermediate-frequency observations (26–68 MHz) were made using the (now nonexistent) 300 foot (91 m) radio telescope at Green Bank by Anantharamaiah, Erickson, & Radhakrishnan (1985). Ershov et al. (1984, 1987) and Lekht, Smirnov, & Sorochenko (1989) have observed these lines in the frequency range 39–118 MHz using the low-frequency array at Pushchino, Russia. Payne, Anantharamaiah, & Erickson (1989, hereafter PAE89) have observed these lines in the frequency range 34–325 MHz using the 140 foot (43 m) and 300 foot telescopes at Green Bank, and more recently (Payne, Anantharamaiah, & Erickson 1994) at frequencies near 566 and 775 MHz. Sorochenko & Walmsley (1991) have observed the lines near 1420 MHz. Finally, Anantharamaiah et al. (1994, hereafter AEPK) have mapped the C272α line emission at 332 MHz over the face of Cas A using the Very Large Array (VLA) and compared the spatial distribution of the recombination line with that of H I and molecular line data. At these low frequencies, Cas A is such a strong source that the diffuse galactic nonthermal background is negligible by comparison. This means that beam dilution effects can be ignored, and that all of these observations, made with widely varying beam sizes, can be compared directly with each other and with model calculations.

The interpretation of the Cas A recombination line observations (Ershov et al. 1984, 1987; PAE89; Konovalenko 1990; Sorochenko & Smirnov 1990; Sorochenko & Walmsley 1991) has revolved around two alternative models: (1) a cold gas

model, in which the hydrogen is probably molecular, and (2) a warm gas model, in which the hydrogen is the atomic gas seen in absorption at $\lambda 21$ cm. (Models in which the gas is both cold and atomic, and hence strongly absorbing at $\lambda 21$ cm, imply very large densities and pressures. Allowing the cold gas to be molecular decouples the recombination and $\lambda 21$ cm absorption lines, so that this problem can be avoided.) One of the attractive features of the warm gas model is the wealth of physical parameters that can be derived if the recombination lines and $\lambda 21$ cm absorption lines originate in the same gas. These parameters are robust, in the sense that they do not depend on the unknown details of the distribution of the gas across the face of Cas A. These physical parameters are sufficient to constrain the heating and cooling rates in the gas, and to determine an equilibrium temperature. A successful equilibrium model would (1) match the observed line broadening as a function of principal quantum number n, (2) match the observed variation of integrated optical depth with n, (3) be in thermal balance, and (4) have a pressure consistent with the appropriate phase of the interstellar medium (ISM). A warm gas model should have a pressure consistent with the cold neutral phase of the ISM: neither so low as to permit only a warm ($\sim$8000 K) neutral phase nor so high as to be far from pressure balance.

The fit of both warm and cold gas models to the observations has not been very satisfactory. In terms of a fit to the data, the cold gas models predict that the integrated optical depth in the line stays relatively constant at the lowest frequencies, in good agreement with the reported results, while the warm gas models predict that it increases at the lower frequencies. On the other hand, the cold gas models predict that the integrated optical depth at 566 MHz should be at least five times that observed near 230 MHz, but it is actually about the same. In terms of the derived physical parameters (PAE89), both models implied pressures much higher than the typical interstellar pressure, and the warm model seemed to have insufficient heating to maintain the model temperature, using the thermal models of Draine (1978).

There have been a number of developments since the discussion in PAE89. First, the VLA observations by AEPK have shown that the distribution of the carbon recombination line emission over the face of Cas A corresponds more closely to the distribution of H I than that of molecular gas. This suggests an association of the C II region with the atomic hydrogen, as assumed in the warm gas models. Second, we have obtained from Dr. Walmsley the computer code used to calculate both the warm gas model presented in Walmsley & Watson (1982) and cold gas models. This code has a long history and has been the basis for much of the interpretive work in the field of radio recombination lines. The basic method goes back to Brocklehurst (1970) and much of the code dates back to at least 1977 (Brocklehurst & Salem 1977). Results for hydrogen were presented by Salem & Brocklehurst (1979), and earlier papers referred to therein. Walmsley & Watson (1982) added the dielectronic-like process described by Watson, Western, & Christensen (1980) to this code. This process involves the fine structure transition ($^2P_{1/2} \rightarrow {}^2P_{3/2}$) in the ground state of singly ionized carbon. Our use of this code allows us to vary the physical parameters of the models while maintaining a match to the primary constraint: the observed line broadening at low frequencies. Third, following Shull & Woods (1985) and Verstraete et al. (1990), we have performed calculations to find the equilibrium temperature of a cloud, given the physical parameters inferred by combining the fitted model parameters with $\lambda 21$ cm results. This allows us to judge whether the model is physically reasonable. The most significant difference from the thermal balance calculations of Draine (1978) is the addition of heating by polycyclic aromatic hydrocarbon (PAH) molecules. Details are given in Appendix B. Fourth, and finally, plasma physicists (e.g., Hummer & Mihalas 1988; Gulyaev & Nefedov 1989, 1991) have given serious thought to nonideal plasma effects that prevent atoms from having bound states at principal quantum numbers above some critical n_{cr}. This research leads to a change in the boundary condition at large n when calculating level populations. We have modified the computer code to calculate departure coefficients for this new class of models, and compare the results with the observations.

We begin, however, with a critical examination of the data. In § 2 we compare model profiles with published spectra and find that both the line width and the line intensity at the lowest frequencies have been underestimated. In § 3 we refine the discussion of PAE89 by calculating models like those presented in Walmsley & Watson (1982) and comparing them to the corrected data. We find that no cold model fits the corrected data. And while there are warm models that adequately fit the recombination line data, they fail the thermal balance and pressure checks. The problem lies in the level population calculations. In § 4 we consider the physical processes that disrupt atomic states with large principal quantum number n and select the proper boundary condition for model calculation. The best-fitting new models may have too little line broadening at low frequencies, but otherwise fit the recombination line and neutral hydrogen data with physical conditions typical of the cold neutral interstellar medium. Our model is in thermal balance at a pressure allowing pressure balance with the warm neutral phase of the ISM. PAH molecules appear to be the dominant heat source in both neutral phases.

2. THE OBSERVED DATA

The higher frequency observations (PAE89; AEPK) have resolved the Cas A carbon recombination line spectrum into three components at velocities of -1.2, -37, and -48 km s^{-1}, as in the case of H I and molecular lines. These velocities correspond to the Orion and Perseus arms in the direction of Cas A. At these frequencies, the peak line intensities of the three features are roughly in the ratio 2:3:9, respectively. The only other detection of the Orion arm feature is at 25 MHz by Konovalenko (1990). We have not attempted a fit to the Orion arm feature since available data are sparse.

The observed quantities that we attempt to model are the line width and the integral of the optical depth across the line: $\int \tau(v)dv$. In order to have a consistent set of data spanning the entire observed frequency range, we treat the Perseus arm feature as a single component. The width of the lines increases dramatically toward lower frequencies due to pressure and radiation broadening, and it becomes increasingly difficult to separate the two Perseus arm features (-37 and -48 km s^{-1}) below 50 MHz ($n > 500$). At the higher frequencies, we obtain an integrated optical depth by adding the contributions of the two Perseus arm features. We have used the integrated optical depth as tabulated by Sorochenko & Smirnov (1990). In Figure 1, we have plotted in integrated optical depth in the -48 km s^{-1} feature as open squares, and the -37 km s^{-1} feature, scaled up by a factor of 2, is shown as triangles. Although points at some values of n differ by many σ, the overall distribution of points seems consistent with a single dependence of integrated optical depth on principal quantum number n.

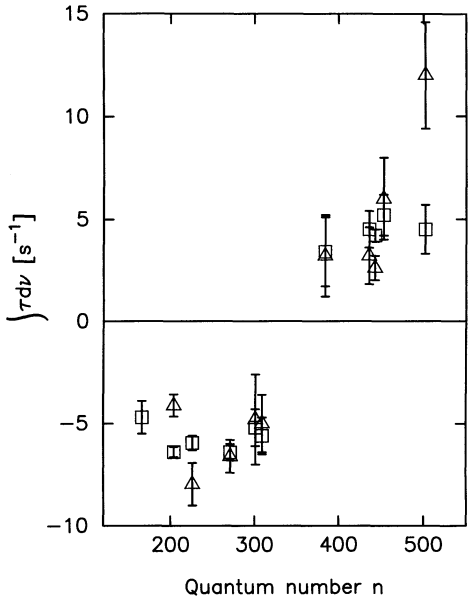

FIG. 1.—A comparison of the frequency dependence of the integrated optical depth in the two Perseus arm velocity components. The −48 km s^{-1} data are shown as squares, and the −37 km s^{-1} data, scaled up by a factor of 2, are shown as triangles. The variation with principal quantum number n is sufficiently similar that we consider it reasonable to compare the sum of these two features with the blend observed at lower frequencies.

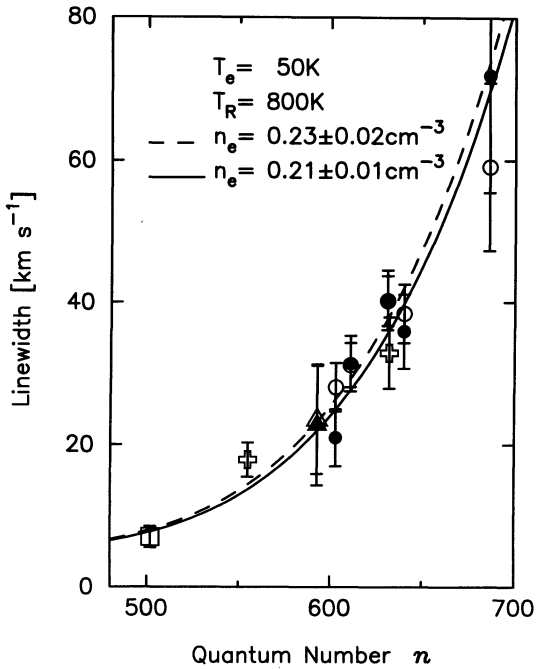

FIG. 2.—Plot of the width of the −48 km s^{-1} feature as a function of principal quantum number n. The open circles are from Konovalenko (1984), the open squares are from PAE89, the open triangle is from Lekht, Smirnov, & Sorochenko (1989), and the open crosses are from Anantharamaiah, Erickson, & Radhakrishnan (1985). The filled circles are the Konovalenko (1984) points corrected for baseline subtraction (see text), and the filled triangle is the Lekht, Smirnov, & Sorochenko (1989) point, similarly corrected. The solid and dashed curves are the best fit of eq. (1) to the corrected and uncorrected widths, respectively.

Therefore, it is reasonable, as a first approximation, to consider the sum of the two Perseus arm velocity components as a single feature directly comparable to the line blend observed at lower frequencies.

The line width consists of a Doppler component, with a Gaussian line shape, and a component due to pressure and radiation broadening, with a Lorentzian line shape. The result is a Voigt profile. At low frequencies the line shape should be nearly Lorentzian, while at high frequencies it should be nearly Gaussian. Following Ershov et al. (1984), the width of the Voigt profile is approximated as

$$\Delta\nu_L = 0.53L + \sqrt{0.22L^2 + D^2}\,, \qquad (1)$$

where D is the Doppler, or Gaussian width, and L is the Lorentzian width. The details of calculating L can be found in Appendix A. To summarize, Griem (1967) showed that interactions of electrons with the line emitters can be treated in the sudden or impact approximation, where only initial and final states need to be considered, rather than in the quasi-static approximation, where the details of the interaction must be known. In the impact approximation, L is inversely related to the level lifetime, or proportional to Γ, the rate at which the level is depopulated. This is simply a result of the uncertainty principle. The dominant contributions to Γ are induced radiative and collisional transitions, which correspond to radiation and pressure broadening contributions to L, respectively. In contrast to PAE89, we calculate Γ using transition rates from the departure coefficient calculation rather than using the formulas in Shaver (1975). This leads to higher estimates of the electron density.

In Figure 2, we show the dependence of line width ΔV, in km s^{-1}, on principal quantum number n. Observations with $n > 440$, and those observations with $n < 550$ which did not resolve the two velocity features, are not shown. We performed a weighted least-squares fit of equation (1) to the open symbols and to the four data points with $n < 300$. For a radiation temperature at 100 MHz of 800 K, spectral index of −2.6, and electron temperatures of 20, 50, and 100 K, the best-fitting electron densities are 0.35, 0.23, and 0.15 cm^{-3}, respectively. The statistical 1 σ error on the fitted electron density is typically about 10%.

We used these parameters to model expected line profiles. The models consist of the sum of three Voigt profiles, centered at −48, −37, and −1.2 km s^{-1}, with heights in the ratio 9:3:2, and Doppler widths corresponding to full widths at half-maximum (FWHM) of 3.9, 5.9, and 2.2 km s^{-1}. The result is then smoothed to the velocity resolution of the observations by convolving the model with a sin x/x response function whose width (FWHM) is 1.2 times the spectrometer channel spacing—this is the appropriate response function for unsmoothed data from a digital autocorrelation spectrometer, like those of Konovalenko (1984, 1990). This model provides an adequate fit to the high-frequency profile shapes, provided that small shifts in the velocity scales of the observed spectra are allowed. This is illustrated in Figure 3, where the model profile is compared to the C444α profile, seen in absorption at 75 MHz, and the C272α profile, seen in emission at 325 MHz. The spectra are from PAE89.

The model profile for $n = 640$ is shown in Figure 4 as the solid curve which peaks at a value of unity. The ripples on the curve are due to sidelobes in the response function (and there is also an edge effect). The velocity scale was chosen to match

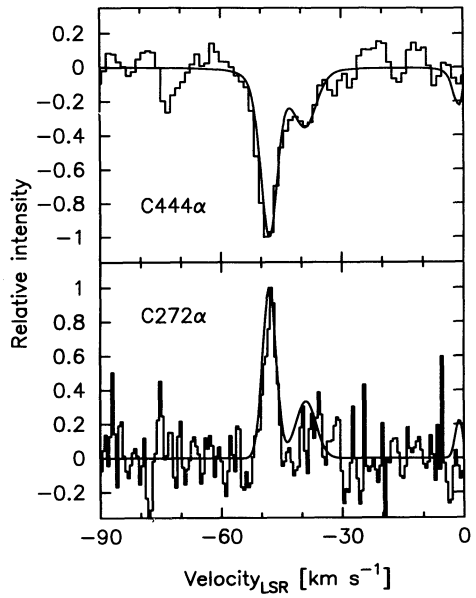

FIG. 3.—Normalized profiles from PAE89 shown with model profiles generated just as the one in Fig. 4. The model profiles provide an adequate representation of the observed profiles without the addition of any broad features that might be present in a two-component model of the cloud.

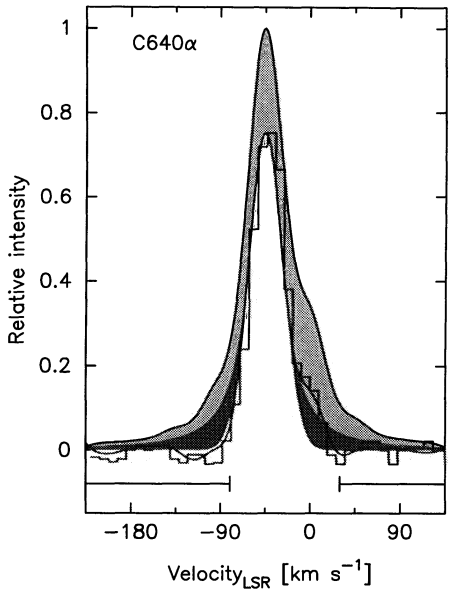

FIG. 4.—A model C640α line. The velocity range is chosen to match the published profile of Konovalenko (1984). The upper envelope of the shaded region is the expected profile for physical condition that give the best fit to the observed line broadening as a function of n. The lower solid curve represents the "observed" profile, obtained by subtracting a baseline from the expected profile. The horizontal bars beneath the spectrum show the velocities used for fitting the baseline. The dark shaded region indicates the correction to the area under the line made by Sorochenko & Smirnov (1990), but we suggest that the appropriate correction includes all of the shaded area.

that of the published profile (Konovalenko 1984). The published profile is the result of a long integration and appears almost noiseless. The observed spectrum drops to zero intensity well within the observed band, but the model profile has only dropped to about 2% of the peak at the edges of the band, suggesting that baseline subtraction has removed the broad wings. We removed a baseline from our model profile by fitting a sixth-order polynomial to the edges of the model profile, forcing zero crossings near the velocities of those in the published profile. A lower order fit left residuals above the noise in the published profile. The region of the spectrum used for baseline fitting is indicated in Figure 4 by the horizontal bars below the spectrum. The result of baseline subtraction is the lower solid curve in the figure. The histogram is the observed spectrum, normalized to the same peak intensity as the baselined model. The similarity between the baselined model and the observation is striking, including even the spurious ripples introduced into the baseline by the baseline removal process (although this is true only for sixth-order baseline fitting). Konovalenko (1984) does not describe the steps used to obtain the final spectrum, but we have no reason to doubt that baseline removal—a standard procedure in radio spectroscopy—has been applied to these data.

The width of the observed $n = 640$ profile appears to be due to a combination of line blending, instrumental resolution, and baseline removal, in addition to the combination of Doppler width and line broadening described by equation (1). In the case of the model profile shown in Figure 4, the physical parameters determined from fitting equation (1) to the observed line widths result in a model profile that is too wide. The observed width is reproduced if the electron densities are reduced by about 30%, to 0.29, 0.18, and 0.13 cm^{-3} for temperatures of 20, 50, and 100 K, respectively.

We repeated our analysis on the other spectra shown in Konvalenko (1984), except for the $n = 732$ profile, and on the $n = 593$ spectrum shown by Lekht et al. (1989). Results depend on the order of the fit and the velocities selected for fitting the baseline, but in each case we used the lowest order baseline that produced residuals with the noise of the published profile, and selected velocities so that the model Gaussian coverages to zero at velocities near those of the published profiles. For each spectrum, we determined the electron density that reproduced the observed line width after baseline removal. These electron densities were then used to calculate a width consisting of contributions from a Doppler width and line broadening alone, eliminating the effects of line blending, baseline removal, and instrumental resolution.

The corrected widths are listed in Table 1 and shown in Figure 2 as filled symbols. These corrected widths are essentially the result of a deconvolution of the two Perseus arm velocity components under the assumption of a constant 3:1 ratio in line heights and identical contribution to line broadening, both as a function of principal quantum number. Since neither of these assumptions is likely to be correct, even though there is no clear evidence that they are not, the results must be considered somewhat more uncertain than the widths derived from the observations themselves. Nevertheless, we performed

TABLE 1

CORRECTED LINE PARAMETERS

Frequency (MHz)	Transition	Corrected ΔV (km s^{-1})	Corrected $\int \tau\, dv$ (s)	Original Reference
20.3	C686α	71.9 ± 16.4	32.1 ± 10.1	1
25.0	C640α	35.9 ± 5.2	27.8 ± 3.6	1
26.1	C631α	40.3 ± 4.2	23.9 ± 3.7	1
28.8	C611α	31.4 ± 3.9	14.8 ± 5.3	1
29.9	C603α	21.0 ± 4.0	13.3 ± 2.4	1
31.5	C593α	22.8 ± 8.8	22.7 ± 7.6	2

REFERENCES.—(1) Konovalenko 1984; (2) Lekht, Smirnov, & Sorochenko 1989.

a weighted fit of equation (1) to these corrected widths. The solution is shown as the solid curve in Figure 2. For electron temperatures of 20, 50, and 100 K, the best-fitting electron densities are decreased slightly from their original estimates to 0.32, 0.21, and 0.14 cm^{-3}, respectively.

We now turn to the effect of baseline removal on integrated optical depth. As shown in Figure 4, baseline subtraction causes the area under the line to be significantly underestimated. The shaded areas, and their extrapolations to large velocities, correspond to the areas removed by baseline subtraction. In this case, the shaded area, even after subtracting out the Orion arm feature, is slightly more than the area under the "observed" profile, meaning that over 50% of the area has been lost. In their tabulation, Sorochenko & Smirnov (1990) applied a correction to the observed area assuming that the observers had accurately measured the height and width, but of a Gaussian rather than a Voigt profile. Their correction corresponds to the dark shaded areas in Figure 4. Still, because baseline correction has reduced both the height and width of the profile, and actual area appears to be nearly 50% greater than that of the "corrected" area. A similar analysis was performed for the other spectra shown in Konovalenko (1984) and for the spectrum shown in Lekht et al. (1989), and these values are used below for comparison with model calculations. Our adjusted values are listed in Table 1.

The result of this correction to the integrated optical depths can be seen in Figure 5, where the dependence on n is shown. Our corrected values for the Konovalenko (1984) and Lekht et al. (1989) points are again shown as filled circles and a filled triangle, respectively. All of the other points are plotted with the values tabulated by Sorochenko & Smirnov (1990). Data from PAE89 are shown as open squares, and the value from our VLA spectrum is shown as hexagram. The open pillow-shaped symbols are from Payne et al. (1994). The open diamond is from Ershov et al. (1984), and the open stars are from Ershov et al. (1987). Upper limits from PAE89 and Ershov et al. (1984) are indicated by the filled triangles. (The curves are discussed in a subsequent section.) We have chosen not to use the data of Anantharamaiah Erickson, & Radhakrishnan (1985) because of doubts concerning the calibration. There has been considerable uncertainty whether the integrated optical leveled off at large n or continued to increase. It now seems likely that the integrated optical depth continues to increase with n up to the highest n yet observed.

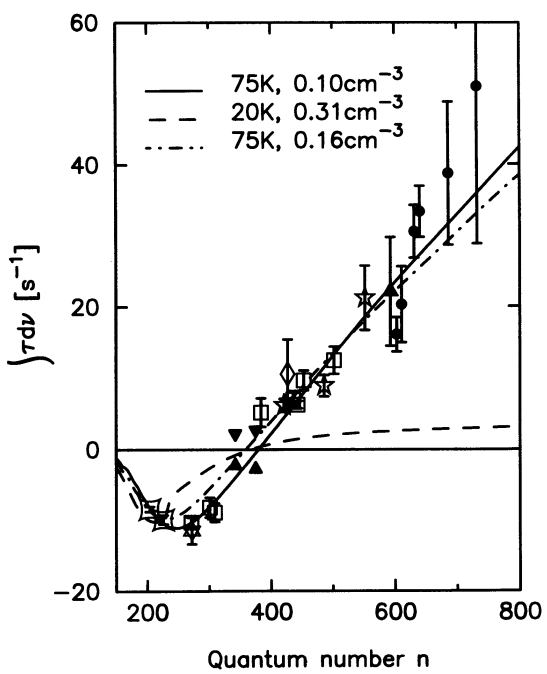

FIG. 5.—Observed integrated optical depths are compared to WW-type model predictions. Models are labeled by their electron temperature and density. The filled points have been corrected for the effects of baseline subtraction. References for the plotted points are given in the text. The solid line is the best-fitting WW model, for which the radiation temperature is $T_R = 1600$ K. The dashed line is a typical cold gas model, indicative of the failure of such models to fit the data. Warm models with $T_R = 800$ K all fail to fit the points near $n = 300$, as shown by the dash-dotted curve.

3. MODELING THE DATA

In this section, we describe the process of matching predicted line intensities to the data. For this purpose, we need to calculate the integrated optical depth in the line as a function of principal quantum number n. Because the line formation process takes place under conditions not in thermodynamic equilibrium, the relative level populations of the atoms in the gas must be calculated from theory. The result of this calculation is a set of departure coefficients b_n and β_n, where b_n is the ratio of the actual population of atoms with an electron in level n to thermodynamic equilibrium value,

$$b_n = [n]/[n]_{\rm LTE} \, . \tag{2}$$

and where

$$\beta_n = 1 - \frac{kT_e}{h\nu} \frac{d}{dn} (\ln b_n) \, . \tag{3}$$

The product $b_n \beta_n$ is the factor by which recombination lines are amplified above their thermodynamic equilibrium intensity.

The calculation proceeds by assuming that the rate at which each quantum level is depopulated is equal to the rate at which is the repopulated from other levels (Brocklehurst 1970). Radiative and collisional processes for changing the quantum numbers of bound electrons, as well as ionization and recombination processes, must be considered. A boundary condition is imposed at low n and at high n. The high n boundary condition is applied by matching the calculation to an asymptotic solution obtained analytically for the hydrogenic case, assuming an infinite number of levels populated according the thermodynamic equilibrium, i.e., $\lim_{n\to\infty} b_n = 1$. The basis for this nonphysical assumption is that collisional level-changing processes will dominate over radiative processes at large n, leading to the conclusion that the level populations will be thermalized. Although it was clear (e.g., Brocklehurst & Seaton 1972) that there must be some n_q such that there are no discrete states for $n > n_q$, it was thought that the effect of this assumption would be small for $n \ll n_q$.

In the case of carbon, the departure coefficients also depend on the relative populations of the $^2P_{1/2}$ and $^2P_{3/2}$ fine structure levels of singly ionized carbon—only ions with electrons in the lower state may participate in the dielectronic-like recombination process described by Watson et al. (1980). If the density is low, then collisional excitation of the upper level is balanced by radiative de-excitation and the emission of a $\lambda 158$ μm photon (an important cooling process). If the density is higher,

then collisional de-excitation begins to compete with radiative de-excitation, and the level populations begin to approach their thermodynamic equilibrium values. Following Watson et al. (1980) and Ponomarev & Sorochenko (1992), we define R as the correction factor for the ratio of the fine structure level populations:

$$R \equiv \frac{[n(^2P_{3/2})/n(^2P_{1/2})]}{[n(^2P_{3/2})/n(^2P_{1/2})]_{\rm LTE}} = \frac{n_e\gamma_e + n_{\rm H}\gamma_{\rm H}}{n_e\gamma_e + n_{\rm H}\gamma_{\rm H} + A_r} . \quad (4)$$

Here γ_e and $\gamma_{\rm H}$ are the de-excitation rates due to collisions with electrons and hydrogen atoms, respectively, and $A_r = 2.4 \times 10^{-6}$ s^{-1} is the spontaneous radiative decay rate. We used $\gamma_{\rm H} = 5.8 \times 10^{-10} T_e^{0.02}$ cm^{-3} s^{-1} (Tielens & Hollenbach 1985) and $\gamma_e = 4.51 \times 10^{-6} T_e^{-1/2}$ (Hayes & Nussbaumer 1984; effective collision strength from Keenan et al. 1986). We assumed that all of the electrons come from carbon, so that we could compute the atomic hydrogen density given the electron density, the cosmic abundance of carbon $A_{\rm C} = 4.0 \times 10^{-4}$ (Morton 1974), and $\delta_{\rm C}$, the carbon depletion factor, or abundance of carbon as a fraction of the cosmic abundance: $n_e = \delta_{\rm C} A_{\rm C} n_{\rm H}$.

In practice, the Salem & Brocklehurst (1979) computer code calculates the level populations for a small number of "pivotal" levels, up to some maximum $n_{\rm max}$. The results reported by Walmsley & Watson (1982) used 75 pivot points and $n_{\rm max} = 10^3$. We modified the code to allow for more pivot points and for $n_{\rm max}$ to be as large as 10^4, and repeated the Walmsley & Watson (1982) calculations with $n_{\rm max}$ set to 2500 and 4500. In the hydrogenic cases, the results were essentially unchanged. In the dielectronic case, however, there were significant differences between the $n_{\rm max} = 1000$ and $n_{\rm max} = 4500$ cases when we chose physical parameters appropriate to the warm gas model. Derived emission measures differed by as much as 25% near $n = 600$. Calculated b_n differed significantly from unity at $n = n_{\rm max}$ when $n_{\rm max} = 1000$. Our final results were calculated with $n_{\rm max} = 1000$. Our final results were calculated with $n_{\rm max} = 10^4$. We will refer to models calculated with $n_{\rm max} = 10^4$, $\lim_{n\to\infty} b_n = 1$, and including dielectronic effects as Walmsley & Watson (1982) or WW-type models. We will refer to models calculated without dielectronic effects as hydrogenic, Salem & Brocklehurst (1979), or SB models.

Once departure coefficients are calculated we can predict the line optical depth integrated over frequency, given in terms of the model parameters as

$$\int \tau_{\rm Cn}\, dv = 2.046 \times 10^6 T_e^{-5/2} \times \exp\left(\frac{1.58 \times 10^5}{n^2 T_e}\right) {\rm EM_C}\, b_n \beta_n \ {\rm s}^{-1} . \quad (5)$$

The only unknown is ${\rm EM_C} = n_e n_{\rm C^+} l$(cm^{-6} pc), the emission measure of the carbon line, where l is the path length through the cloud (pc). We determined the emission measure by performing a weighted least-squares fit of equation (5) to the data. The upper limits were not included in the fit.

Each model calculation begins with a choice of electron and radiation temperatures. We considered models with electron temperatures between 16 and 150 K, and a range of radiation temperatures. The radiation temperature as seen by the cloud can have any value from 800 K, which is the galactic background level is this direction, to one-half of the brightness temperature of Cas A, depending on the distance between the cloud and Cas A. The electron density is then obtained from a fit to the corrected line widths. We typically ran models in which carbon was undepleted, depleted to half its cosmic abundance, and depleted to one-third its cosmic abundance.

All of the cold gas WW-type models predict that the integrated optical depth near $n = 200$ is 4–5 times that at high n, rather than the other way around, as the corrected data indicate. A typical example is shown as the dashed curve in Figure 5. $T_R = 800$ K for this model. Cold gas models predict that the integrated optical depth increases very little with increasing n, and may actually decrease at high n, while the corrected data show a steady increase. We conclude that there is no cold gas WW model that fits the observed data points. This is consistent with the AEPK suggestion that the recombination lines do not originate in a molecular cloud.

The WW model with $T_e = 75$ K and $T_R = 800$ K provides quite a good fit to the data. This model is shown as the dash-dotted curve in Figure 5. The fit can be improved by decreasing the electron density while increasing the radiation temperature, to maintain the amount of line broadening. The best fitting WW model has $T_R = 1600$ K and is shown as the solid curve in Figure 5. The model parameters are listed in Table 2, where this is model A.

As discussed in PAE89, the attractive feature of the warm gas models is that the carbon line region can be identified with the H I λ21 cm absorption-line region. Combining recombination line data with neutral hydrogen data allows a detailed probe of physical conditions within the region. We reexamine the physical conditions within the cloud in light of the new model parameters, still considering the -48 and -37 km s^{-1} features as a single, homogeneous cloud. We use the same numbers as PAE89 for the neutral hydrogen: spin temperature $T_S = T_e$, and column density $N_{\rm H} = 4.4 \times 10^{21}$ (T_e/100 K) cm^{-2}. Due to the strong saturation of the λ21 cm absorption lines, this column density is quite uncertain. As described in Payne, Salpeter, & Terzian (1983), the neutral hydrogen spin temperature is not necessarily the physical temperature of any parcel of gas, and should be considered an upper limit to the physical temperature in the gas which causes the absorption.

The emission measure obtained from the best-fitting warm gas WW-type model is 0.0198 ± 0.0007 cm^{-6} pc, compared to 0.0084 cm^{-6} pc in PAE89. Assuming that all electrons come from carbon, i.e., $n_e = n_{\rm C^+} = 0.101$ cm^{-3}, the emission measure

TABLE 2

BEST-FITTING MODEL PARAMETERS

	Model	
	A	B
	Departure Coefficients	
Parameter	WW	Present
n_e (cm^{-3})	0.101	0.05
T_e (K)	75	35
T_R (K)	1600	800
$n_{\rm cr}$	...	4450
Emission measure (cm^{-6} pc)	0.0198 ± 0.0007	0.0056 ± 0.0003
$n_{\rm H}$ (cm^{-3})	550	221
Pressure p/k (cm^{-3} K)	41,400	7,740
$\delta_{\rm C}$	0.46	0.6
Fractional ionization x	$<5 \times 10^{-5}$	$<6 \times 10^{-5}$
Ionization rate $\zeta_{\rm H}$ (s^{-1})	$<6 \times 10^{-17}$	$<8 \times 10^{-17}$
PAH abundance $A_{\rm PAH}$	5.4×10^{-7}	4×10^{-7}
Thermal balance $T_{\rm eq}$ (K)	31	36
Cooling time t_T (yr)	800	1390

and electron density imply a path length of 1.9 pc. Dividing the neutral hydrogen column density by the path length implies a space density $n_H = 550$ cm^{-3}. This model was calculated with a carbon depletion factor $\delta_C = 46\%$, chosen to be consistent with the derived depletion factor found by comparing the carbon (i.e., electron) density to the derived neutral hydrogen density. The implied thermal pressure is $p/k = 4.1 \times 10^4$ cm^{-3} K, 10 times higher than the typical interstellar value of $\sim$4000 cm^{-3} K (e.g., Kulkarni & Heiles 1987). As explained in PAE89, the pressure derived this way depends on the ratio of recombination line to neutral hydrogen optical depths and does not depend on the fraction of Cas A covered by the cloud.

The absence of detectable hydrogen recombination lines provides a constraint on the proton density n_p, and on the hydrogen ionization rate ζ_H (Shaver 1976). The most sensitive upper limit to the hydrogen recombination lines is that of Konovalenko (1990) at 25 MHz: $\tau_{H639\alpha} < 7 \times 10^{-5}$. We used a synthetic profile to convert from a peak optical depth to an integrated optical depth, and found $\int \tau_{H639\alpha} dv < 0.5$ s^{-1}. However, our hydrogenic departure coefficient calculation with model A physical parameters predicts a crossover between emission and absorption at the frequency, leaving the emission measure unconstrained. If we take the weaker PAE89 upper limit $\tau_{H300\alpha} < 0.56 \times 10^{-3}$, and use a synthetic profile to convert to integrated optical depth, we find $\tau_{H300\alpha} dv < 3.0$ s^{-1}. The hydrogenic departure coefficient calculation predicts $b_{300}\beta_{300} = -12.3$, which implies an emission measure EM < 0.0059 cm^{-6} pc. Comparison with the emission measure for carbon listed in Table 2 implies $n_p/n_{C^+} < 0.3$, and hence that $n_p/n_e = n_p/(n_p + n_{C^+}) < 0.23$, and $n_p/n_H < 5 \times 10^{-5}$. At least 75% of the electrons come from carbon, since abundances rule out a significant contribution from other metals. From equation (6) in PAE89, which compares the recombination line and λ21 cm absorption line peak optical depths, we find for the -48 km s^{-1} feature $\zeta_H < 6 \times 10^{-17}$ s^{-1}.

It is difficult to avoid the high pressure derived for model A. By lowering the temperature, we could reduce the column density of neutral hydrogen required to produce the observed λ21 cm absorption. But this would require increasing the electron density or the radiation temperature, to maintain the observed line broadening. To obtain a good fit while raising the electron density requires a decreased emission measure, resulting in much shorter path lengths through the cloud and even higher pressure. We might have overestimated the neutral hydrogen column density, and could lower the pressure by taking a lower estimate. However, it could be decreased by only a factor of 2 before requiring carbon to be undepleted; any further reduction would require raising the hydrogen ionization fraction above the observed limit.

A second conclusion is that model A is far from being in thermal balance. The details of evaluating the thermal balance are given in Appendix B. Imposing the upper limits on the hydrogen fractional ionization and ionization rate derived above, the equilibrium temperature is only 31 K. Decreasing the pressure by a factor of 2 and allowing carbon to be undepleted, assuming that the neutral hydrogen column density is overestimated, still gives an equilibrium temperature of 31 K. If we take all of the carbon missing from the gas phase and put it in PAH molecules, to maximize the heating rate, we can get the temperature up to only 59 K. (If there is no heating by PAH molecules, then the equilibrium temperature is only 21 K.) The cooling time for these models is under a thousand years. All of the WW models, when fitted to the data, have equilibrium temperatures between 30 and 38 K, and short cooling times. And all of the models with electron temperatures in this range give a poor fit to the data. We conclude that there is no single component WW model that will fit the data and satisfy the thermal balance criterion.

Sorochenko & Walmsley (1991), facing the problem of fitting WW models to the data, considered models with both a warm and a cold component. Our revision of the line strengths at large n has largely removed the need for a cold component, however, since the warm component itself now provides such good agreement. The best-fitting linear combination of model A and a cold model has essentially no contribution from the cold model. Still, it is reasonable to consider models where some of the carbon line emission measure arises in the outer layer of a molecular cloud. As explained by Sorochenko & Walmsley (1991), at a boundary between atomic and molecular regions there should be a transition zone where the hydrogen is molecular and the carbon is still completely ionized.

In search of a two-component model, we found that it was fairly easy to generate models that fit our new observations at $n = 204$ and $n = 226$, along with all of the data with $n > 400$. These models all give absurdly large pressures if combined with the neutral hydrogen data, and to avoid this we would like them to be associated with the molecular cloud. We therefore looked for complementary models that would contribute to the emission lines near $n = 300$ but contribute little elsewhere. One hint that this may be reasonable is that the line widths of the features with n between 300 and 450 are unexpectedly large, as shown in Figure 6, which may indicate that they do not originate in the same gas as the lines at both smaller and larger n. These models would not be constrained by the line broadening at large n, and could perhaps be arranged to give a reasonable pressure in the neutral gas. But this does not seem to work—there are no models that peak near $n = 300$. The only models that fit the points near $n = 300$ are those, like model A, that also fit the high n points, and so there appears to be no room for a second component.

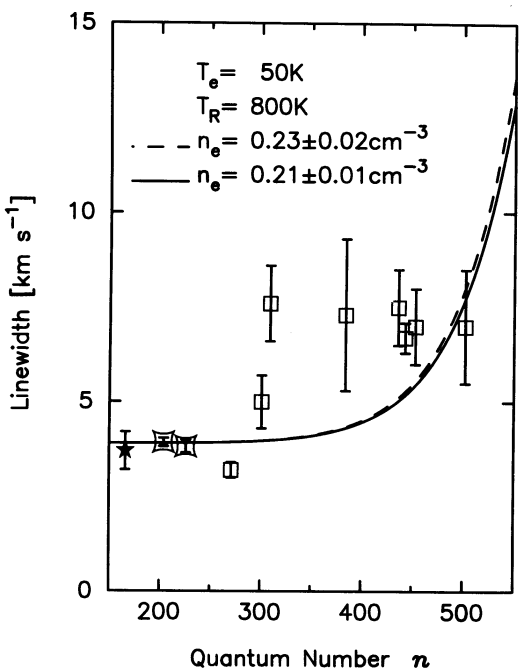

FIG. 6.—A detailed look at Fig. 2 showing the unexpectedly large line widths of features with n between 300 and 450. This may indicate that two physical components are present.

We are forced to conclude that there is no WW-type model that satisfies all four of our criteria. Either these clouds are ephemeral objects, far from equilibrium—in which case the thermal balance and pressure checks are irrelevant—or there is something wrong with the theory used to interpret the data. We consider this second possibility in the next section.

4. A NEW CLASS OF MODELS

In the previous section, we mentioned that the Brocklehurst (1970) type calculation used a boundary condition at large n based on the assumption of an infinite number of levels, populated according to thermodynamic equilibrium, so that $\lim_{n\to\infty} b_n = 1$. Although it was clear that at some large n the levels must be empty, it was thought that the effect of this assumption would be small at the n of interest. In recent years, significant progress has been made in understanding how nonideal plasma effects affect the highly excited states (Hummer & Mihalas 1988; Gulyaev 1990), and it is now possible for level population calculations to include a more physically meaningful treatment of the boundary condition at large n. In the case of the Cas A data, at least, these new models lead to very different conclusions about the physical conditions in the gas.

There have been a number of attempts to describe the process that Hummer & Mihalas (1988, hereafter HM) refer to as the truncation or convergence of the internal partition function, i.e., the mechanisms that limit an atom to a finite number of bound states. Brocklehurst & Seaton (1972) and Shaver (1975) mention the blending of levels at high n. However, this does not lead to a prescription for calculating the level populations. HM and Gulyaev & Nefedov (1989, 1991) mention an effective lowering of the atomic ionization potential as a description used by earlier workers, and then go on to describe the problems with this description. HM argue for an approach in which the convergence of the internal partition function is the result of a smooth decrease in the occupation probability of states at high principal quantum number. Nonideal plasma effects perturb these states, reducing the probability that an electron could remain bound in them. By avoiding discontinuities in the level populations of the atoms, it is possible to describe the free energy of the plasma as a differentiable function, allowing the equation of state to be determined by minimizing the free energy. The thermodynamic properties of the plasma can be computed in a consistent way. The disruption of high n states due to interactions with the plasma also provides a physically plausible explanation for pressure ionization. Occupation probabilities are calculated from the physics of the particle interactions. HM consider interactions with neutral and charged perturbers in the quasi-static and impact approximations. If more than one type of interaction is present, their corresponding occupation probabilities are simply multiplied together.

We point out that HM are primarily interested in physical conditions relevant to stellar envelopes and interiors. The success of the occupation probability formalism in reproducing the results of laboratory spectroscopic observations of plasmas has been demonstrated by, for example, Däppen, Anderson, & Mihalas (1987). And the formalism has been applied successfully to astronomical observations—in the determination of white dwarf masses by Bergeron, Saffer, & Liebert (1992), for example. Although the stellar envelope conditions are very different from those of the cold, very neutral, atomic phase of the ISM, the latter is still well characterized as a partially ionized plasma. The significant difference is that the perturbing charged particles of interest are the ions in the stellar envelope case, but are the electrons in the ISM case. In a hot stellar envelope, the free electrons form a completely degenerate gas. The electrons are moving so fast that the cross section for collision is extremely small, and the electrons cause electric field fluctuations that are too rapid to have any quasi-static effects. In the ISM case, collisions with electrons dominate over collisions with ions since the latter move so slowly. It turns out that translating the relevant physics from the stellar envelope regime to the ISM regime is almost as simple as changing all of the subscripts from "ion" to "electron." One reason for this is that in both cases the perturbers are uncorrelated—the Coulomb energy of two charged particles at their mean separation is small compared to their thermal kinetic energy. This allows the treatment of quasi-static plasma effects to be similar. Another reason is that the thermal speed of a proton at a temperature of 10^5 K is about the same as that of an electron at 50 K, allowing the treatment of impacts to be similar. Translating § 4.2.3 of HM, concerning perturbations by charged particles in the quasi-static approximation, yields expressions essentially identical to those in Gulyaev & Nefedov (1989).

The first demonstration of the relevance of the truncation of the internal partition function to low-frequency recombination lines was provided by Gulyaev & Nefedov (1989, hereafter GN). Examination of equations (3) and (5) reveals that the line intensity crosses through zero when $d \ln b_n/dn = h\nu/kT_e$. In the Salem & Brocklehurst (1979) calculation, b_n increases asymptotically toward unity, and the crossover typically appears at large n ($n > 500$) as the slope becomes small. The observation that the crossover occurs at $n \sim 350$ in the Cas A data leads to the conclusion that the temperature must be low. The dielectronic-like effects on carbon recombination lines introduced by Watson et al. (1980) allowed WW to obtain a qualitatively different solution: the "lifetime-lengthening" of states with n of a few hundred increase their population, as shown in Figure 9, and leads to a local maximum and change of sign in $d \ln b_n/bn$ and β, provided that the temperature is high enough for the effect to be present. However, the boundary condition $\lim_{n\to\infty} b_n = 0$ alone implies that β will change sign. GN showed that this boundary condition, and a reasonable choice of physical parameters, were sufficient to predict a crossover near $n = 350$, as observed, without invoking the dielectronic-like effects. Although their choice of physical parameters implies that the dielectronic-like effects should be present, this is still a remarkable result.

The physical process that GN invoke for reducing the occupation probability of states at high n is ionization by the fluctuating electric field felt by an atom at some position in the plasma. The objection to this calculation is that it is made in the quasi-static approximation. HM show that this treatment is not valid for perturbations by electrons unless the temperature is much lower than 10 K. Otherwise, the field fluctuations are too rapid to be treated quasi-statistically. To calculate the effect of perturbations by electrons in the impact approximation, we are guided by § 4.3 in HM. The physical mechanism is basically the same as pressure broadening: an atom exists in state n only for the time t between successive inelastic collisions with electrons. Times t will have a Poisson distribution with characteristic time equal to the inverse of the level depopulation rate Γ: $P(t)dt = \Gamma \exp(-\Gamma t)dt$. This level will have an energy uncertainty Δ_n such that $t\Delta_n > \hbar/2$. We drop the factor of 2 to avoid imposing the minimum uncertainty. Intuitively, a state for which the energy uncertainty is comparable to its ionization energy χ_n will have a decreased occupation probability. We therefore take the occupation

probability to be the cumulative probability that a state has a lifetime greater than $\hbar/\chi_n$:

$$w_{n,e} = \int_{\hbar/\chi_n}^{\infty} \Gamma \exp(-\Gamma t) dt = e^{-\hbar\Gamma/\chi_n} . \quad (6)$$

we define n_{cr} to be that value of n for which the occupation probability is reduced to e^{-1}. Therefore, n_{cr} is the principal quantum number for which

$$\hbar\Gamma(n_{cr})/\chi_{n_{cr}} = 1 . \quad (7)$$

At very large n, Γ (eq. [A3]) should be dominated by collisions, since the radiation field will turn over at low frequencies ($\nu < 1$ MHz, $n > 1900$). At large n, the Gee et al. (1976) collision rate goes as $\Gamma \approx 2 \times 10^{-4} n^4 n_e T_e^{-3/2} \ln(nT_e)$ s^{-1}, and $\chi_n = 2.18 \times 10^{-11} n^{-2}$ ergs. Therefore,

$$n_{cr,e}^6 \approx 6 \times 10^{20} \frac{T_e^{3/2}}{n_e} \frac{1}{\ln(nT_e)} \quad (8)$$

and

$$n_{cr,e} \approx 1930 \frac{T_e^{1/4}}{n_e^{1/6}} \quad (9)$$

for temperatures of interest.

We must also consider the interaction with neutral particles, meaning hydrogen atoms. The physical mechanism, again, as described in HM, is that interactions with neutral particles will start to lower the occupation probability of excited states having a characteristic radius r_n larger than the mean neutral interparticle separation—i.e., for states whose volume is large enough to encompass or "touch" neutral particles. Neglecting the volume of the neutral perturbers, and taking $a_0 n^2$ as the characteristic radius for principal quantum number n, the occupation probability is (HM's eqn. [3.13])

$$w_{n,\text{neutral}} = \exp\left(-\frac{4\pi}{3} a_0^3 n^6 n_H\right) . \quad (10)$$

If, as in the previous section, we take $n_e = \delta_C n_H/2500$, then

$$n_{cr,\text{neutral}} = 10830(1/n_H)^{1/6} , \quad (11)$$

$$n_{cr,\text{neutral}} = 2940(\delta_C/n_e)^{1/6} . \quad (12)$$

Since the total occupation probability is the product of the electron and neutral interaction probabilities just determined, we end up taking the smaller of $n_{cr,e}$ and $n_{cr,\text{neutral}}$. For temperatures above 10 K, as long as the fractional ionization of hydrogen is small, $n_{cr,\text{neutral}}$ will be slightly smaller than $n_{cr,e}$.

We modified the WW computer code to calculate departure coefficients with the new boundary condition. This consisted primarily of replacing the statistical weight g_n with an effective statistical weight $g_n^* = w_n g_n$, where w_n is the occupation probability, and changing the boundary condition at large n to $\lim_{n\to\infty} b_n = 0$. For this paper, we have taken the GN approach of using a simple step function for the weights:

$$w_n = \begin{cases} 1, & n < n_{cr} , \\ 0, & n > n_{cr} . \end{cases} \quad (13)$$

Taking the GN value of n_{cr}, and omitting dielectronic effects, our calculations agree with the departure coefficients calculated analytically by GN. Given our simplified approach to the occupation probabilities, determining the proper boundary condition reduces to the problem of calculating n_{cr}. The multiplicative property of occupation probabilities means that we need only consider the process that leads to the smallest n_{cr}.

A comparison of the results of our hydrogenic calculation with those of SB is shown in Figure 7. All of the curves are calculated with an electron temperature $T_e = 50$ K, but with electron densities of 1.0, 0.1, 0.01, and 0.001 cm^{-3} for the solid, dashed, dash-dotted, and dotted curves, respectively. The top panel shows the SB results. All of the curves converge to the same asymptote at small n, where the level populations are determined primarily by spontaneous transitions and so are independent of density. And the curves all converge at large n to the boundary condition $b_n = 1$, which corresponds to collisionally controlled level populations. The transition between the two asymptotes occurs at smaller n for higher electron densities because collision rates are higher. The situation is more complicated in our calculation, shown in the lower panel. The behavior at small n is nearly identical to the SB case. But a large n, the program is being cut off at a value of n_{cr} which increases as the electron density is decreased. GN showed (their eq. [16]) that the asymptotic form of these solutions is

$$b_n = 6.46 \times 10^6 n_e T_e^{-1/2} n^{-1.63} . \quad (14)$$

So the curves with smaller electron densities have longer and shallower "tails" at large n. The effect of forcing a change in n_{cr} is shown in Figure 8. The solid curve shows a model for which $T_e = 50$ K and $n_e = 0.09$ cm^{-3}, for which equation (11) implies $n_{cr} = 4000$. The other two curves show the result of forcing a factor of 2 difference in n_{cr}, leaving all other parameters unchanged. The change does propagate down to the range of observations, making it important to get the physics right. The quasi-static calculation, for example, would correspond to values of n_{cr} less than half as large as the ones we used (eq. [4.42] in HM), leading to differences in the results as large as those shown in Figure 8.

The addition of the Watson et al. (1980) dielectronic-like effects is shown in Figure 9. Each of these models was calculated for $n_e = 0.1$ cm^{-3}, $T_e = 50$ K, $T_R = 800$ K, and $R = 0.1$.

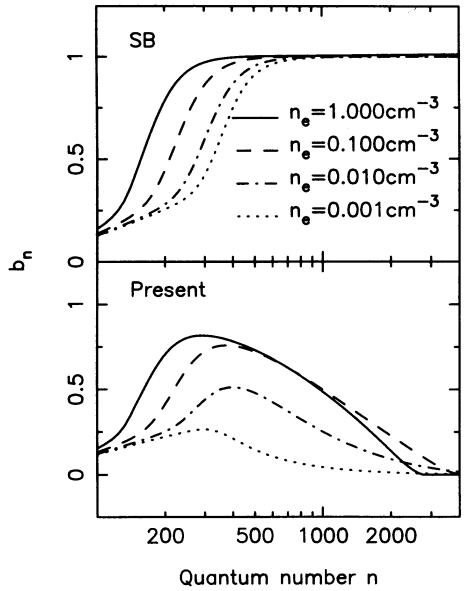

FIG. 7.—A comparison between Salem & Brocklehurst (SB, 1979) departure coefficients b_n and the current results, calculated in the occupation probability formalism. These calculations are "hydrogenic," meaning that the dielectronic-like effects introduced by Watson, Western, and Christensen (1980) are not included. Each model was calculated with an electron temperature $T_e = 50$ K and electron density as indicated.

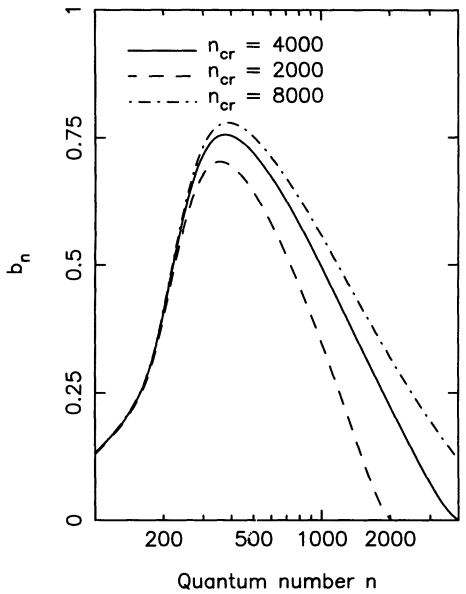

FIG. 8.—The solid curve is a calculation where eq. (11) implies $n_{cr} = 4000$. The other two curves show the effect of forcing a factor of 2 change in n_{cr}, leaving other parameters unchanged.

The SB model and the WW model both assume $\lim_{n\to\infty} b_n = 1$, but differ by the addition of dielectronic effects to the latter. The lifetime-lengthening effect that the dielectronic-like process of Watson et al. (1980) has on level populations is to create a bottleneck for cascading electrons, increasing the level populations at n of a few hundred. Our models assume that $\lim_{n\to\infty} b_n = 0$. The very high n levels are empty, so there are fewer cascading electrons to be caught in the bottleneck, and the backup does not extend as high, moving the peak to lower n. Even the hydrogenic model implies absorption lines at intermediate n ($n \sim 300$–400).

We did not find any new models that fit the integrated optical depths using electron densities determined by line broadening. As was the case for the WW models, the only models that fit the points with $n \sim 300$ have electron densities too small to provide observed line broadening if the radiation temperature is $T_R = 800$ K. A typical model with the electron density determined from the line width is shown in Figure 11 as a dashed line. The solid line is a best-fitting model, described below. Model C640α profiles generated with the best-fitting model parameters have widths that are only 80% of the observed, corrected widths. This descrepancy could be due to errors in the collision rates, where the uncertainties are estimated to be 20% (Gee et al. 1976). There is additional uncertainty implied by the approximate equality symbol in equation (A2), estimated to be a factor of 2 (Brocklehurst & Leeman 1971).

In the WW models, it was possible to recover the observed line widths by increasing the amount of radiation broadening, but that is not possible with our models. The difference is the boundary condition at large n. If increasing the intensity of the radiation field speeds up the cascade to lower levels, then the level populations will simply be smaller—there is no infinite source of electrons at higher n to make up for the loss. This is illustrated in Figure 10, where the lower four curves show the decrease in level populations over a range of radiation temperatures. The upper two curves are the WW models at the extremes of this temperature range. The sensitivity of the WW models to the value of the radiation temperature is clearly much less than in our models. If we lower the WW model A radiation temperature to $T_R = 800$ K, the model profile widths

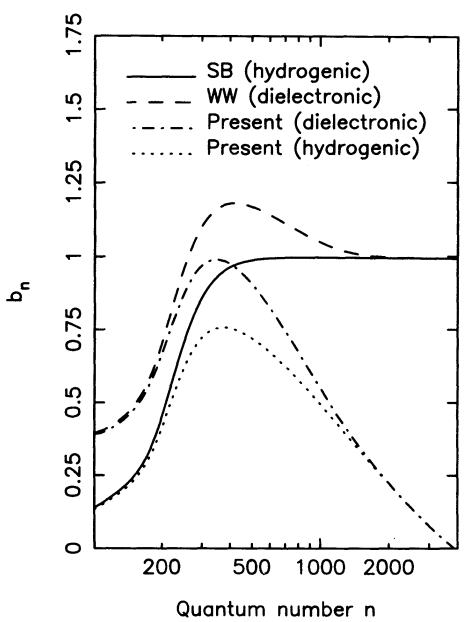

FIG. 9.—A comparison of different methods for calculating the departure coefficient b_n. Each of these models was calculated for $n_e = 0.1$ cm^{-3}, $T_e = 50$ K, $T_R = 800$ K, and $R = 0.1$. Models are labeled "dielectronic" if they include the dielectronic-like effects introduced by Watson, Western, & Christensen (1980), and "hydrogenic" if they do not. The first two models are calculated in the manner of Salem & Brocklehurst (SB, 1979) and Walmsley & Watson (WW, 1982). For our model, $n_{cr} = 3860$.

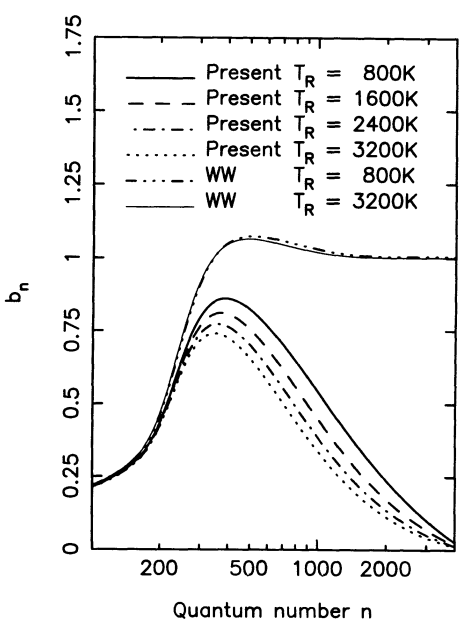

FIG. 10.—An illustration of the effect of varying the radiation temperature T_R. For each model, $n_e = 0.05$ cm^{-3}, $T_e = 35$ K, and $\delta_C = 0.5$. The lower four curves show that in our model there is a significant drop in level populations as T_R increases. Increasing the radiation temperature allows induced radiative transitions to empty a level faster, and there is no source of electrons at high n to make up for the loss. In contrast, the upper two curves show that WW models are much less sensitive.

are about 90% of the observed, corrected widths—a smaller discrepancy than for our models. In view of our limited understanding of the Cas A recombination line regions, we are inclined to accept the discrepancy in line widths for the moment, and hope for a resolution in the future.

Lifting the constraint imposed by line broadening, our best-fitting model is shown as the solid curve in Figure 11. This may appear to be a better fit than the best-fitting WW model, but the χ^2 is actually a bit higher. The parameters derived from this model and the neutral hydrogen data are listed in Table 2 as model B. The derived hydrogen density is $n_H = 205$ cm^{-3}, and the derived pressure, $p/k = 7200$ cm^{-3} K, is well within the range of normal interstellar pressures. So our third criterion is satisfied—the recombinations could plausibly originate in the same gas as the λ21 cm absorption lines.

A cold gas model is shown as the dash-dotted curve in Figure 11. The fit is not nearly as bad as in the WW case. In fact, a good fit to the emission lines can be obtained if the electron density is small enough (e.g., $T_e = 20$ K and $n_e = 0.05$ cm^{-3}). But this does not solve the line width problem. These cold models will have narrow lines at high n. They would still contribute most of the observed optical depth at high n, leaving little room for a contribution from wide lines. There are warm gas models that are complementary to the cold models, contributing to the adsorption lines at high n but not to the emission lines at low n. But in the best-fitting linear combination of warm and cold models, shown in Figure 12, it is the cold, narrow component that dominates at large n. The warm component has a pressure $p/k > 10^5$ cm^{-3} K. So, neither the cold gas model nor a two-component model gives satisfactory results.

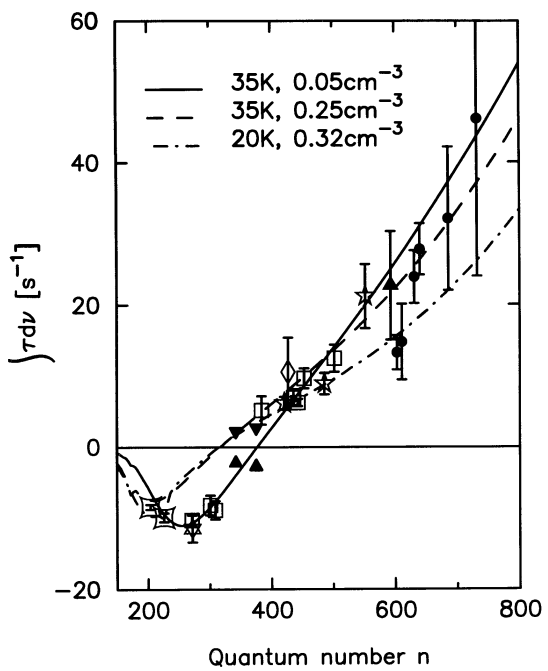

FIG. 11.—Our best-fitting model (*solid curve*), and a typical model having an electron density determined from line broadening (*dashed curve*). As with the WW models, fitting the points near $n = 300$ requires electron densities too low to provide the observed line broadening. The best-fitting model, model B in Table 2, implies a reasonable pressure in the λ21 cm absorbing neutral hydrogen, and is in thermal balance, satisfying the other requirements for a successful model. A typical cold gas model is also shown (*dash-dotted curve*).

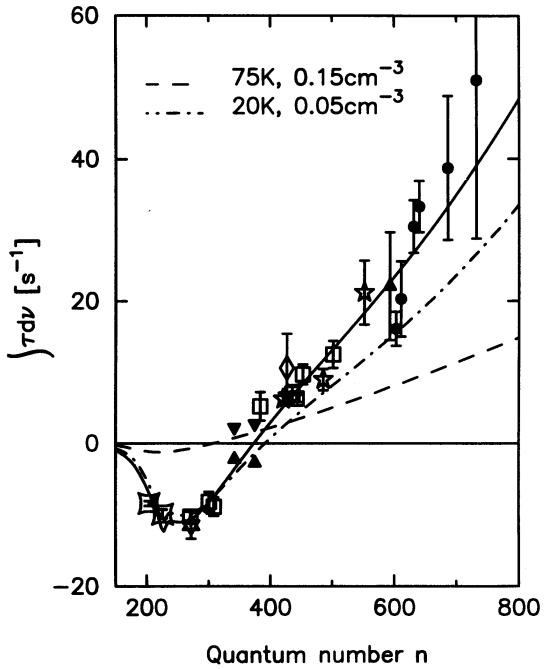

FIG. 12.—The solid curve is the best-fitting sum of typical warm and cold gas models. The cold gas component, shown separately as the dash-dotted curve, has a small electron density in order to fit the points near $n = 300$. The warm component (*dashed curve*) would provide the broad lines at large n but it is the cold component that dominates at large n. The pressure in the warm component is very high: $p/k > 10^5$ cm^{-3} K. So neither a cold model nor a two-component model gives a satisfactory result.

Our hydrogenic departure coefficient calculation with model B parameters predicts $b_{300}\beta_{300} = -5.2$. Repeating the calculation from the previous section, the absence of a hydrogen H300α recombination line implies an emission measure EM < 0.0021 cm^{-6} pc. Therefore $n_p/n_{C^+} < 0.35$, $n_p/n_e < 0.26$, and $n_p/n_H < 6 \times 10^{-5}$. Comparison of recombination line and λ21 cm optical depths implies $\zeta_H < 8 \times 10^{-17}$ s^{-1}. To consider the thermal balance, we allow 20% of the carbon missing from the gas phase to be in PAH molecules, implying $A_{PAH} = 4 \times 10^{-7}$ (we assumed 80 carbon atoms per PAH molecule). These parameters are sufficient to predict thermal balance at a temperature $T_{eq} = 36$ K, so the model is in thermal balance. The hydrogen ionization rate has such a low upper limit that it makes almost no contribution to heating the gas. Setting the ionization rate to zero lowers T_{eq} by only 0.2 K. On the other hand, setting the abundance of PAH molecules to zero lowers T_{eq} to 25 K. The importance of heating by PAH molecules is clearly demonstrated. Under model *B* conditions PAH molecules provide two-thirds of the total heat input, more than twice the contribution due to photoelectric heating by grains, and 50 times the contribution due to cosmic rays.

The model B physical parameters determine a point on the pressure versus temperature phase diagram of the gas. By making small adjustments to the hydrogen density, and then iteratively recalculating the hydrogen ionization balance and the thermal balance until they are consistent, the rest of the phase diagram can be calculated. The result is shown in Figure 13. The cross marks the model B point. The curves are for different values of the PAH abundance, A_{PAH}, while retaining the ionization rate, ζ_H, and carbon depletion, δ_C. The darkest curve is the canonical PAH abundance, obtained by putting

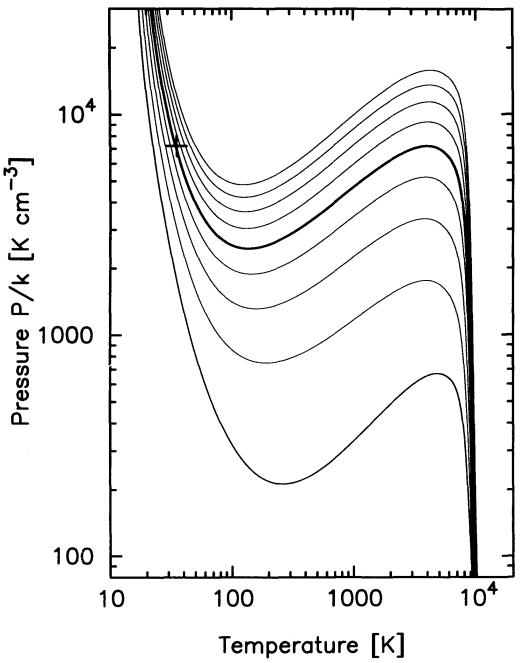

FIG. 13.—A family of pressure vs. temperature phase diagrams. The cross marks the position of model B. The input parameters for each curve are the primary ionization rate $\zeta_H = 8 \times 10^{-17}$ s^{-1} and a carbon depletion factor of $\delta_C = 0.6$. The abundance of PAH molecules is zero for the lowest curve, and increases in steps of 1×10^{-7} for each higher curve. The darkest curve, at $A_{PAH} = 4 \times 10^{-7}$ is the model B value.

20% of the carbon missing from the gas phase into PAH molecules. Portions of the curve with positive slope are thermally unstable. Model B can be in pressure balance with a hot gas model (but just barely) having a temperature of 4000 K. At this temperature, PAH's contribute three-quarters of the total heat input.

In conclusion, there is a model which appears to underestimate the observed line broadening, but otherwise provides a good fit to the carbon recombination line integrated optical depths, is consistent with the hydrogen recombination line and λ21 cm neutral hydrogen data, has a temperature safely below the measured spin temperature, has a pressure that allows balance with the other phases of the interstellar medium, and is in thermal balance. This is remarkable for a model that depends on the observed column density of neutral hydrogen and only two free parameters: the electron temperature T_e and density n_e. The carbon depletion factor δ_C is a crucial input parameter since it sets the neutral hydrogen density n_H, which enters the departure coefficient calculation through n_{cr} (eq. [11]) and R (eq. [4]). But it is also a derived quantity, and so must be chosen to be self-consistent, and to fall into the narrow range of astrophysical interest: $0.2 < \delta_C < 1$. Once the carbon depletion factor is set, all other properties follow: (1) the neutral hydrogen density n_H, and hence the pressure, (2) the gas-phase abundance of carbon, and therefore the cooling rate, and (3) the abundance of PAH molecules, A_{PAH}, which sets the heating rate. The thermal balance check is straightforward. There are many ways for a model to fail, so it is satisfying to find a model that does a pretty good job of satisfying all of the constraints.

The use of the occupation probability formalism has led to some interesting conclusions. The most interesting may be that the physical parameters associated with our model B are not at all exotic—instead, they are typical of a widespread component of the ISM. This leads us to a few words of caution. Although the physical mechanisms for truncating the atomic partition function translated quite transparently from the stellar to the interstellar regimes, the resulting critical quantum numbers differ by almost three orders of magnitude (being only of order 10 in the stellar case). This leaves a lot of room for processes that we have not considered, for quantum mechanical effects, or for inappropriate approximations. And the occupation probability was incorporated into our calculations in a very crude manner, violating the spirit that motivated the formalism in the first place. So further investigation is required, into both the theory and the mechanics of the calculation. The calculation also needs to be extended into other physical regimes, including H II regions and the warm ionized medium.

5. DISCUSSION

In the Introduction, we described the four tests for judging a model to be successful: explaining (1) line width versus principal quantum number n, (2) integrated line optical depth versus n, (3) a reasonable pressure deduced from neutral hydrogen absorption data, and (4) thermal balance. The line width turned out to be a problem, with the best-fitting models predicting lines only 80% as wide as the observed lines. In WW models the observed widths can be recovered by increasing the amount of radiation broadening, but not in our models. Given our limited knowledge of the Cas A recombination line regions, we are unsure whether our best-fitting models satisfy the line width constraint or not.

The WW models do not appear to satisfy simultaneously all of the last three criteria. The recombination lines cannot originate in a molecular cloud and still have the observed dependence of line strength on principal quantum number n. So, the lines must originate in the atomic gas, allowing us to combine the recombination line and λ21 cm line results. But this combination does not allow the cloud to be in equilibrium: fitting the line strengths implies temperatures near 75 K, but the ensemble of fitted parameters indicates that the temperature would be nearer 30 K. The situation is not improved by allowing the recombination lines to originate in both molecular and atomic regions. Of course, the cloud really could be far from equilibrium—failing our checks does not discredit this possibility.

The question of whether the HM occupation probability formalism should be incorporated into the SB and WW departure coefficient calculations is not to be decided by seeing if it improves the fit to the data. Our improved understanding of the relevant physics implies that it must be included. As it turns out, however, the Cas A carbon recombination lines provide a demonstration that making this change leads to a very different physical picture. Instead of a high-pressure region far from thermal balance, we find physical conditions typical of the cold neutral medium. Through a combination of radio observations we have a very detailed description of the conditions in these clouds that are 3 kpc away. Conditions are so typical that the importance of heating by PAH molecules, clearly required for the Cas A clouds, may be a general feature of the neutral phases of the ISM, as first suggested by d'Hendecourt & Léger (1987).

The spatial correspondence of C272α and H I optical depths observed by AEPK suggested to us that the recombination lines and the λ21 cm absorption arise in the same gas, and that

a single model should suffice to explain both sets of data. The fact that we found such a model, with very typical properties, implies that it may be possible to detect recombination lines of carbon from many other directions. Although there have been several searches (Konovalenko 1984; Anantharamaiah, Payne, & Erickson 1988; Golynkin & Konovalenko 1990), lines have been detected in only a few directions and the observed lines are much weaker than in the direction of Cas A. What is special about this line of sight? What makes these clouds so relatively conspicuous?

The critical factor appears to be the low temperature. There is a strong explicit dependence on temperature in the integrated optical depth (eq. [5]). In contrast, the departure coefficients and emission measure depend only weakly on temperature. When we consider a feature with a given λ21 cm H I optical depth, and assume pressure balance with the ISM, the hydrogen column density N_H is proportional to the temperature, since cold gas absorbs more efficiently, but the space density n_H is inversely proportional to T, to maintain the pressure balance. Therefore the path length l goes as T^2. But the electron density is proportional to the hydrogen density, and so the emission measure EM $= n_e{}^2 l$ is independent of T. So the change in predicted line strength is due almost entirely to the factor of $T^{-5/2}$ in equation (5). A 50% increase in temperature corresponds to a decrease in line strength by almost a factor of 3.

To consider a particular case, Payne, Salpeter, & Terzian (1983) failed to detect a C274α recombination line from the optically thick H I cloud seen in absorption against the extragalactic continuum source 3C 123. The neutral hydrogen column density seen in absorption is $N_H = 1.0 \times 10^{21} T/60$ K cm^{-2}. If we assume a typical pressure of $n_H T_e/k = 4000$ cm^{-3} K, and take the temperature to be only 35 K, we would deduce a hydrogen density of $n_H = 114$ cm^{-3}. To keep the gas at this temperature would require a PAH abundance $A_{PAH} \sim 2.5 \times 10^{-7}$, which, as above, corresponds to a gas-phase carbon depletion factor $\delta_C \sim 0.75$, and hence to an electron density of $n_e = 0.034$ cm^{-3} and an emission measure EM ~ 0.0019 cm^{-6} pc. Our new departure coefficients imply an integrated optical depth of 6.4 s^{-1} or 0.006 km s^{-1}. Assuming a Gaussian line shape with a width of 5.7 km s^{-1} implies a peak optical depth of $\sim 1.1 \times 10^{-3}$, which would have been detected easily. However, repeating this argument with $T = 50$ K predicts a feature at the 3 σ level, and taking $T = 60$ K, as implied by the emission-absorption data, predicts an undetectable feature.

Analyses of the Arecibo λ21 cm emission-absorption surveys have remarked on the correlation between the apparent temperature of the absorbing gas and the optical depth (Dickey, Salpeter, & Terzian 1978; Payne et al. 1983; and Colgan, Salpeter, & Terzian 1988). The sense of the correlation is that the higher optical depth features appear to be colder. The subject has been brought up again recently by Braun & Walterbos (1992), who plot the data in a way that does not compress the high optical depth end of the correlation. It is interesting that the equilibrium temperature of 36 K for the Cas A features is about what the correlation would predict, based on their λ21 cm optical depths. These clouds are the highest optical depth H I clouds in the galaxy, and yet they appear to have typical physical properties. The failure to detect recombination lines from the high optical depth cloud seen toward 3C 123 can be understood as a temperature effect implying significant cloud-to-cloud variations in temperature. And if lower optical depth clouds really are warmer, that could explain why low-frequency recombination lines have been so hard to detect along other lines of sight. The Cas A recombination lines, then, like the Cas A λ21 cm absorption lines, would represent one extreme of a broad distribution of ISM properties rather than a unique observation.

We would like to thank Dr. S. A. Gulyaev for bringing his work to our attention. And we are very grateful to the referee for a careful reading of the manuscript and for many insightful, constructive comments.

APPENDIX A

LINE BROADENING

The width of radio recombination lines has been a subject of careful study. Griem (1967) examined the interaction of ions and electrons with the emitting atoms and concluded that the interactions could be treated in the sudden or impact approximation, where only initial and final states need to be considered, rather than in the quasi-static approximation, where the details of the interaction must be known. This should be true for transitions throughout the radio region, even if the temperature is low. For conditions of interest here, the temperature is too low to use the line widths derived by Griem (1967), but Baranger's (1958) theory of pressure broadening by electron impacts is still applicable. Baranger (1958) used the optical theorem to write the width L (related to the imaginary part of the scattering amplitude) in terms of the total cross sections of the initial and final states:

$$\pi L = \tfrac{1}{2} n_e \left\{ v \left[\sigma_i^{\rm in} + \sigma_f^{\rm in} + \int | f_i(\Omega) - f_f(\Omega) |^2 d\Omega \right] \right\}_{\rm av} , \tag{A1}$$

where v is the electron velocity, $\sigma^{\rm in}$ is the inelastic part of the total cross section, and $f(\Omega)$ is the elastic scattering amplitude, shown here integrated over all scattering angles Ω. The indicated average is an average over a Maxwellian velocity distribution. Following Brocklehurst & Leeman (1971) we assume that cancellation makes the elastic scattering term negligible, and that $\sigma_i^{\rm in} \approx \sigma_f^{\rm in}$. Following Shaver (1975), we replace the inelastic cross section with Γ, the total rate for depopulating a level, to obtain

$$L \approx \frac{\Gamma}{\pi} , \tag{A2}$$

where

$$\Gamma = \sum_{m<n} A_{n,m} + \sum_m (B_{n,m} I_\nu + C_{n,m}) + C_{n,i} . \tag{A3}$$

Here $A_{n,m}$ is the Einstein coefficient for spontaneous emission from level n to level m, $B_{n,m}$ is the coefficient for induced transitions, I_ν is the intensity of the radiation field at the frequency of the transition, $C_{n,m}$ is the rate for collisional transitions from level n to level m, and $C_{n,i}$ is the collisional ionization rate from level n. At large n, this sum is dominated by the sum over $C_{n,m}$, which we associate with pressure broadening, and the sum over $B_{n,m} I_\nu$, which we associate with radiation broadening. Brocklehurst & Leeman (1971) estimate equation (A2) to be accurate to within a factor of 2.

Equation (A2) is basically a restatement of the uncertainty principle. The atom is in a state only for a time $t = 1/\Gamma$, on average. This implies an energy uncertainty Δ such that $t\Delta > \hbar/2$. Following HM, for example, we drop the factor of 2 to avoid insisting on the minimum uncertainty. The energy uncertainty should translate to a line half-width, so $\Delta \sim hL/2$, so we again obtain $L \sim \Gamma/\pi$.

We computed the pressure broadening contribution to equation (A3) due to collisions with electrons using the collision rates calculated by the departure coefficient code. The rates are those given by Gee et al. (1976). Collision rates $C_{n,m}$ were summed over levels m between $n - 40$ and $n + 40$, and the total was divided by π. This procedure results in pressure broadening that is considerably less than that given by equation (64a) in Shaver (1975), used by PAE89. Electron densities must be increased by about 80% to make up for the smaller collision rates. The additional pressure broadening due to collisions with ions was computed from formulae given by Hoang-Binh (1990). The line width is given by

$$\Delta\nu_I = 1.569 \times 10^{-7} Z^{-2} (\mu_i/T_i)^{0.5} n_i F(n, \Delta n)[0.5 + \ln(\rho_{\max}/\rho_{\min})] \text{ kHz} , \tag{A4}$$

for collisions with ions of charge Z, kinetic temperature T_i, and density n_i. The result depends on the reduced mass of the colliding ion-emitting ion system, μ_i. Here, we consider only the effect of collisions with C II ions on the carbon recombination lines, and hence the reduced mass $\mu_i = 6$ amu. We also assume that only carbon ions are present, so that $n_i = n_e$, and that $T_i = T_e$. For α transitions ($\Delta n = 1$), an approximation to function F is given by

$$F(n, 1) = (9/4)n^2[3/2 + 0.271 \ln(2n/3) + 1.92n^{-0.422}] , \tag{A5}$$

and the minimum and maximum impact parameters $\rho_{\min}$ and $\rho_{\max}$, and Debye radius ρ_D are given by

$$\rho_{\min} = 8.301 \times 10^{-5} F(n, \Delta n)^{0.5} (\mu_i/T)^{0.5} , \tag{A6}$$

$$\rho_{\max} = \min [(\pi/2)^{0.5} \lambda/2\pi, \rho_D] , \tag{A7}$$

$$\rho_D = 6.90 \left(\frac{T}{n_i + n_e} \right)^{0.5} . \tag{A8}$$

In these equations, λ is the wavelength of the recombination line. Flannery (1970) has shown that collisions with neutral particles make a negligible contribution to pressure broadening.

Similarly, we computed the radiation broadening contribution to equation (A3) by using the induced transition rates calculated by the departure coefficient code. We summed

$$B_{n,m} I_\nu = W_\nu A_{n,m} \frac{kT_R}{h100 \text{ MHz}} \left(\frac{\nu}{100 \text{ MHz}} \right)^{\alpha - 1} \tag{A9}$$

over levels m between $n - 40$ and $n + 40$, and the total was divided by π. T_R is the equivalent blackbody temperature of the background nonthermal radiation field, measured at 100 MHz, and W_ν is the dilution factor. In all cases, we take $W_\nu = 1$ and assumed a spectral index $\alpha = -2.6$. This procedure results in radiation broadening that is somewhat smaller than that given by equation (65) in Shaver (1975), used by PAE89. In this case, electron densities must be increased by about 10%–15% to make up for the smaller rates.

APPENDIX B

THERMAL BALANCE

To evaluate the possibility that a balance between heating and cooling exists under the physical conditions implied by model fitting, we evaluated the various heating and cooling terms as in Shull & Woods (1985), Draine (1978), and especially Verstraete et al. (1990), who included heating by PAH molecules.

Shull & Woods (1985) begin by calculating an electron density from the ionization balance of species involved. For the purposes of evaluating thermal balance, we simply take the model electron density, and take hydrogen ionization rates ζ_H and fractional ionizations $x = n_{H^+}/n_H$ that satisfy the constraints imposed by the absence of hydrogen recombination lines. (Note that in most references $x \equiv n_e/n_H$.) For the purpose of computing phase diagrams, however, we compute the fractional ionization of hydrogen and helium by balancing recombination with ionization by cosmic rays and collisions with electrons. Ionization by X-rays and collisions with hydrogen atoms are ignored. The procedure is to make an initial guess electron density by adding up the contributions from ionized metals. Then the ionization fractions of hydrogen, and then helium, are determined by iteration.

The overall heating rate Γ may be written as a sum

$$\Gamma = \Gamma_{CR} + \Gamma_g + \Gamma_{PAH} \tag{B1}$$

over contributions from cosmic rays, grains, and PAHs, respectively. We have not included heating by X-rays. The overall cooling rate Λ may also be written as a sum

$$\Lambda = \Lambda_i + \Lambda_{rec} + \Lambda_g + \Lambda_{rad} \tag{B2}$$

over contributions from collisional ionization, recombination, grains, and radiative transitions, respectively. A cloud will be in thermal balance if $\Gamma = \Lambda$.

We write the heating rate due to cosmic rays as

$$\Gamma_{CR} = (1 - x) n_H \zeta E_h(E_0) . \tag{B3}$$

For the heating function per primary ionization E_h, we took a cut through Figure 1 in Shull (1979) at $E_0 = 35$ eV, and crudely fit the dependence on fractional ionization x as

$$E_h = 4.7 + \frac{30}{1 + (\log x/2.3)^4} \text{ eV} . \tag{B4}$$

We calculated Γ_g, the heating due to photoelectric emission from grains, as (Draine 1978)

$$\Gamma_g = \begin{cases} 4.31 + 10^{-5} Y_{PE} Q_{abs} n_H \sigma (1 - u)^{-4} , & 0 < u < 1 , \\ 0 , & u > 1 , \end{cases} \tag{B5}$$

where we have taken values 0.5 for the photoemission yield Y_{PE}, 0.75 for the ratio Q_{abs} of the absorption cross section to the geometric cross section, and 1.5×10^{-21} cm^{-2} for σ, the geometric cross section per hydrogen nucleus (making $n_H \sigma$ the geometric cross section per unit volume). The grain potential u, in units of 5.6 eV, is calculated from equation (15) in Draine (1978).

The heating due to PAH molecules, Γ_{PAH}, was calculated from equation (19) in Verstraete et al. (1990). Using values for the ionization rate of PAHs and for the mean energy of the ejected electron given in Verstraete et al. (1990), we calculate heating rates which are actually somewhat smaller than those shown in their Figure 5. We allow 20% for the carbon missing from the gas phase to be in the form of PAH molecules. Verstraete et al. (1990) allowed 10% of the cosmic abundance of carbon to be in the form of PAH molecules. More recently, Joblin, Léger, & Martin (1992) derived a value of 18%.

Following Shull & Woods (1985), we have included in our calculation the cooling due to the ionization of hydrogen

$$\Lambda_i = n_e n(H^0) \frac{1.27 \times 10^{-21} T^{1/2} \exp(-157800/T)}{1 + T/1.58 \times 10^6} , \tag{B6}$$

and due to recombination of hydrogen

$$\Lambda_{rec} = n_e n_{H^+} \alpha^{(2)} 0.75\, kT , \tag{B7}$$

even though both processes are ineffective at the temperatures are consider here.

The cooling due to collisions with grains, Λ_g, was calculated from equations (9) and (10) in Draine (1978), except that we have not assumed the electron and proton densities to be equal. Therefore, the cooling contribution due to collisions of electrons and protons with grains is

$$\Gamma_{g,e} = \frac{n_H \sigma (2kT)^{3/2}}{(\pi m_e)^{1/2}} \left[s_e n_e (2 + \phi) + n_{H^+} \left(\frac{m_e}{m_H} \right)^{1/2} e^{-\phi} (2\alpha_H + \phi) \right] , \tag{B8}$$

where the electron sticking factor $s_e = 0.5$, and $\phi = eU/kT$.

And finally, our calculation of Λ_{rad}, the cooling rate due to collisionally excited radiative transitions, follows closely the method of Verstraete et al. (1990). We used the same transitions, the same abundances and depletion factors, and the same collisional cross sections. We did allow the depletion factor for carbon, δ_C, to vary, however. And because the density is high in some of our models, we included the effect of collisional de-excitation of the $C^+(^2P_{3/2})$ state.

Spitzer (1978) defines a cooling time t_T, which for these models would be written as

$$t_T = 3/2 n_H k (T - T_{eq})/(\Lambda - \Gamma) . \tag{B9}$$

REFERENCES

Anantharamaiah, K. R., Erickson, W. C., Payne, H. E., & Kantharia, N. G. 1994, ApJ, 430, 682 (AEPK)
Anantharamaiah, K. R., Erickson, W. C., & Radhakrishnan, V. 1985, Nature, 315, 647
Anantharamaiah, K. R., Payne, H. E., & Erickson, W. C. 1988, MNRAS, 235, 151
Baranger, M. 1958, Phys. Rev., 112, 855
Bergeron, P., Saffer, R. A., & Liebert, J. 1992, ApJ, 394, 228
Braun, R., & Walterbos, R. A. M. 1992, ApJ, 386, 120
Brocklehurst, M. 1970, MNRAS, 148, 417
Brocklehurst, M., & Leeman, S. 1971, Astrophys. Lett., 9, 35
Brocklehurst, M., & Salem, M. 1977, Computer Phys. Comm., 13, 39
Brocklehurst, M., & Seaton, M. J. 1972, MNRAS, 157, 179
Colgan, S. W. J., Salpeter, E. E., & Terzian, Y. 1988, ApJ, 328, 275
Däppen, W., Anderson, L. S., & Mihalas, D. 1987, ApJ, 319, 195
d'Hendecourt, L., & Léger, A. 1987, A&A, 180, L9
Dickey, J. M., Salpeter, E. E., & Terzian, Y. 1978, ApJS, 36, 77
Draine, B. T. 1978, ApJS, 36, 595
Ershov, A. A., Ilyasov, Yu. P., Lekht, E. E., Smirnov, G. T., Solodkov, V. T., & Sorochenko, R. L. 1984, Soviet Astron. Lett., 10, 348
Ershov, A. A., Lekht, E. E., Smirnov, G. T., & Sorochenko, R. L. 1987, Soviet Astron. Lett., 13, 8
Flannery, M. R. 1970, ApJ, 61, L41
Gee, C. S., Percival, I. C., Lodge, J. G., & Richards, D. 1976, MNRAS, 175, 209
Golynkin, A. A., & Konovalenko, A. A. 1990, in Radio Recombination Lines: 25 Years of Investigation, ed. M. A. Gordon & R. L. Sorochenko (Dordrecht: Reidel), 209
Griem, H. R. 1967, ApJ, 148, 547
Gulyaev, S. A. 1990, in Radio Recombination Lines: 25 Years of Investigation ed. M. A. Gordon & R. L. Sorochenko (Dordrecht: Reidel), 37
Gulyaev, S. A., & Nefedov, S. A. 1989, Astron. Nach., 310, 403 (GN)
———. 1991, Astron. Nach., 312, 27
Hayes, M. A., & Nussbaumer, H. 1984, A&A, 134, 193
Hoang-Binh, D. 1990, in Radio Recombination Lines: 25 Years of Investigation, ed. M. A. Gordon & R. L. Sorochenko (Dordrecht: Reidel), 51
Hummer, D. G., & Mihalas, D. 1988, ApJ, 331, 794 (HM)
Joblin, C., Léger, A., & Martin, P. 1992, ApJ, 393, L79
Keenan, F. P., Lennon, D. J., Johnson, C. T., & Kingston, A. E. 1986, MNRAS, 220, 571
Konovalenko, A. A. 1984, Soviet Astron. Lett., 10, 353

Konovalenko, A. A. 1990, in Radio Recombination Lines: 25 Years of Investigation, ed. M. A. Gordon & R. L. Sorochenko (Dordrecht: Reidel), 175
Konovalenko, A. A., & Sodin, L. G. 1980, Nature, 283, 360
———. 1981, Nature, 294, 135
Kulkarni, S. R., & Heiles, C. 1987, in Interstellar Processes, ed. D. J. Hollenbach & H. A. Thronson, Jr. (Dordrecht: Reidel), 87
Lekht, E. E., Smirnov, G. T., & Sorochenko, R. L. 1989, Soviet Astron. Lett., 15, 171
Morton, D. C. 1974, ApJ, 193, L35
Payne, H. E., Anantharamaiah, K. R., & Erickson, W. C. 1989, ApJ, 341, 890 (PAE89)
———. 1994, in preparation
Payne, H. E., Salpeter, E. E., & Terzian, Y. 1983 ApJ, 272, 540
Ponomarev, V. O., & Sorochenko, R. L. 1992, Soviet Astron. Lett., 18, 215
Salem, M., & Brocklehurst, M. 1979, ApJS, 39, 633
Schwarz, U. J., Troland, T. H., Albinson, J. S., Bregman, J. D., Goss, W. M., & Heiles, C. E. 1986, ApJ, 301, 320
Shaver, P. A. 1975, Pramana, 5, 1
———. 1976, A&A, 49, 149
Shull, M. J. 1979, ApJ, 234, 761
Shull, M. J., & Woods, D. T. 1985, ApJ, 288, 50
Sorochenko, R. L., & Smirnov, G. T. 1990, in Radio Recombination Lines: 25 Years of Investigation, ed. M. A. Gordon & R. L. Sorochenko (Dordrecht: Reidel), 189
Sorochenko, R. L., & Walmsley, C. M. 1991, A&A Trans., 1, 31
Spitzer, L. 1978 Physical Processes in the Interstellar Medium (New York: Wiley)
Tielens, A. G. G. M., & Hollenbach, D. 1985, ApJ, 291, 722
Torland, T. H., Crutcher, R. M., & Heiles, C. E. 1985, ApJ, 298, 808
Verstraete, L., Léger, A., d'Hendecourt, L., Dutoit, O., & Défourneau, D. 1990, A&A, 237, 436
Watson, W. D., Western, L. R., & Christensen, R. B. 1980, ApJ, 240, 956
Walmsley, C. M., & Watson, W. D. 1982, ApJ, 260, 317 (WW)